Magnetoresistance and Annealing Behaviors of Particulate Co–Au Nanocomposites

Zhanhu Guo,[a,*] Monica Moldovan,[b] David P. Young,[b] Laurence L. Henry,[c] and Elizabeth J. Podlaha[d,,z]**

[a]*Gordon A. and Mary Cain Department of Chemical Engineering, and* [b]*Department of Physics, Louisiana State University, Baton Rouge, Louisiana 70803, USA*
[c]*Department of Physics, Southern University and A&M College, Baton Rouge, Louisiana 70813, USA*
[d]*Department of Chemical Engineering, Northeastern University, Boston, Massachusetts 02115, USA*

$Co_{core}Au_{shell}$ nanoparticles, stabilized with a sulfobetaine surfactant, were fabricated from a displacement reaction of Au^{3+} with Co nanoparticles and compressed into a granular composite. The affect of annealing the composite in a hydrogen environment was investigated and found to have a dramatic effect on the magnetic properties, size, and composition of the CoAu nanoparticles. A negative magnetoresistance was observed and exhibited a parabolic functionality with annealing temperature, increasing and then decreasing with annealing temperature. A similar behavior was observed for the coercivity, attributed to the increase in particle size with the annealing temperature. The surfactant was decomposed with annealing.
© 2007 The Electrochemical Society. [DOI: 10.1149/1.2794685] All rights reserved.

Magnetic metallic nanoparticles such as cobalt[1,2] and iron[3] are of interest due to their potential wide applications, such as biomedical[4] and magnetic storage,[5] arising from their unique physicochemical properties that differ from the corresponding bulk and atomic counterparts.[6] The development of core-shell magnetic nanoparticles has been demonstrated in a variety of systems with a focus on protecting the inner magnetic core from oxidation, which lowers the magnetic moment and limits their applications.[7,8] Shells fabricated with noble metals[9-14] have been reported, using electrochemical methods in both an electroless approach, with an additional reducing agent[12,15,16] added to the solution containing nanoparticles, and via a displacement reaction technique, where part of the core nanoparticle is sacrificed as the reducing agent for the noble metal deposition.[9-11,14] An alternative approach is to create the shell around the nanoparticles in a high-temperature decomposition of organometallic compounds containing the shell element from a co-ordinating solvent, as presented by Fleming et al.,[17] and hence, introducing the effect of temperature to the methodology. Here, we adopt the displacement approach and investigate the influence of heating the resulting core-shell nanoparticles.

A collection of nanoparticles with a nonmagnetic shell surrounding a magnetic core have the potential to exhibit giant magnetoresistance (GMR), a dramatic change of resistance in an applied magnetic field, applicable to sensor materials. The required antiferromagnetic coupling between magnetic particles, such as Co, can occur if the particles are nanometric and separated by a nonferromagnetic layer, such as Au, at the nanometer scale. Multilayered thin films and nanowires with this alternating configuration display GMR. Several reviews on this subject are available.[18-20] Granular alloys, a closely related structure, are bulk or thin-film materials that result in two phases as a consequence of the fabrication process. Often one phase is nanometric and the other surrounds these regions. The granular structure can be thought of as a special form of a collection of nanoparticles. The magnetization orientation of the discrete particles will align parallel to each other by applying a magnetic field to overcome the antiferromagnetic coupling, thus reducing the spin-dependent scattering and the subsequent resistivity. Whereas spin-dependent scattering in layered GMR materials can occur at the interfacial regions of the layers and within the layers, granular materials generally scatter at the interfaces due to the larger surface-to-volume ratio of the magnetic nanoparticulate phases.[21-23]

The factors effecting the extent of GMR include size of the discrete phase,[24] distance between the two magnetic layers (nonmagnetic layer thickness), composition of the granules,[25] shape of the GMR materials which determines the shape anisotropy, and the interface between the particles and the matrix,[26] which can change with annealing as a result of altering the phase separation. Kahn[27] has reported the phase diagram of the cobalt–gold, showing that the gold and cobalt are thermodynamically immiscible; however, metastable CoAu alloys can be fabricated by the electrodeposition method.[28,29] The disadvantage of cluster-based materials is that they typically require high magnetic fields to overcome the anisotropy energy of particles with various shapes and sizes to align their magnetic moments.[30] A collection of compressed nanoparticles, with small size variation, may in principle be used to avoid this limitation. As a step toward this end, there has been a report of a small magnetoresistance (MR) in $Fe_{core}Au_{shell}$ nanoparticles fabricated by the microemulsion method.[12] Our work here furthers this effort and introduces the importance of annealing the core-shell nanoparticles.

Experimental

Synthesis of Co and CoAu nanoparticles.— The precursor cobalt nanoparticles and $Co_{core}Au_{shell}$ nanoparticles were synthesized by the recently reported wet-chemical redox and displacement reaction methods.[10,11,14] A brief description of the procedures is as follows. A mixture of 15 mL superhydride [lithium hydrotriethyl borate, 1 M superhydride tetrahydrofuran (THF) solution] and dodecyldimethyl(3-sulfopropyl)ammonium hydroxide (SB3–12, 0.015 M) in 100 mL THF was added into 100 mL cobalt chloride ($CoCl_2$, 0.0285 M) THF solution and reacted for 1 h under ultrasonic stirring and nitrogen protection. The reaction was quenched by adding ethanol and precipitated by sedimentation. The precipitated cobalt nanoparticles were washed thoroughly with THF and dried under nitrogen flow. The cobalt nanoparticles were then added to a 50 mL $KAuCl_4$ (0.024 M) THF solution under ultrasonication. The gold ions are reduced by the oxidation of the cobalt nanoparticles and the most probable structure is that of a core shell, $Co_{core}Au_{shell}$. In order to prevent the oxidation of the precursor cobalt nanoparticle during Au shell formation, the synthesis was still carried out in a nitrogen protection condition. The initial brown-colored solution changed to blue, indicating that the gold ions oxidized the cobalt surface atoms on the cobalt nanoparticles. The reaction was continued for an additional 1 h. The core-shell nanoparticles were washed thoroughly with THF and dried under nitrogen flow.

In order to study the microstructure effect on the magnetic properties and MR behavior, the prepared $Co_{core}Au_{shell}$ nanoparticles

were annealed at different temperatures, 200, 250, 450, and 600°C, under hydrogen gas (5 vol % hydrogen balanced with argon) flow in a quartz tube situated in a tubular furnace. The annealing temperature was increased to a desired temperature within 30 min and that temperature was maintained for 2 h. The granular alloy sample for the GMR measurement was prepared by the cold-press method. The applied pressure was 5000 psi (Presser model: Carzer Hydraulic 3912) and the pressing duration time was 2 min. A longer pressing time of 10 min (not shown here) did not alter the results.

Characterization.— The morphology of the annealed $Co_{core}Au_{shell}$ nanoparticle was examined by transmission electron microscopy (TEM, JEOL 2010) with an accelerated voltage of 200 kV using bright field. The samples for TEM were prepared by dropping an anhydrous alcohol solution of core-shell nanoparticles on a carbon-coated, holey copper grid. Scanning electron microscopy (SEM, Cambridge S-260) was used to study the sample annealed at 600°C.

The magnetic properties of the annealed $Co_{core}Au_{shell}$ nanoparticle were tested using a superconducting quantum interference design (SQUID) magnetometer (Quantum Design, Inc., model MPMS 5S). The samples for magnetic measurements were prepared in powder form in gelation capsules. The temperature-dependent magnetization was investigated using zero-field-cooled (ZFC) and field-cooled (FC) conditions at an applied field of 100 Oe. ZFC was done by cooling the sample first to 4 K without a field, then magnetization changes were recorded with the temperature increasing from 4 to 300 K with an applied field of 100 Oe. FC was recorded immediately after ZFC by decreasing the temperature from 300 to 4 K with a constant field of 100 Oe. Field-dependent magnetization (hysteresis loop) was tested for two temperatures, 10 and 300 K. To test the oxidative property of the cobalt cores, both the ZF and ZFC methods were carried out.

The physicochemical interaction between the SB3–12 and the freshly prepared $Co_{core}Au_{shell}$ nanoparticles and the existence of the SB3–12 surfactant in the annealed $Co_{core}Au_{shell}$ nanoparticle samples were investigated by Fourier transform infrared (FTIR) spectroscopy (Thermo Nicolet Nexus 670) under transmission mode. The pure surfactants were ground with KBr and compressed into a pellet, and their spectra were recorded as a reference spectrum to be compared with those of the $Co_{core}Au_{shell}$ nanoparticle samples.

Magnetic-field-dependent resistance was measured in a 9 T Quantum Design physical property measurement system (PPMS) measurement system using the standard four-probe ac technique and GMR was calculated by the following equation, $\Delta R/R(0) = \{[R(H) - R(0)]/R(0)\} \times 100\%$, where $R(H)$ and $R(0)$ are the resistance at zero and any applied field of H, respectively. The applied magnetic field is perpendicular to the film, i.e., the applied current.

Results and Discussion

Figure 1 shows (a) a TEM image after preparing the $Co_{core}Au_{shell}$ nanoparticles and (b) the magnetic-field dependent resistance after they are compressed into a pellet without any subsequent annealing. The nanoparticles have an average diameter size of 2.7 nm with a narrow size dispersion in the range of 1–3.3 nm. The selected area electron diffraction (SAED) rings (from the inner to outer) of the as-prepared nanoparticles correspond to lattice spacings of 0.234, 0.204, 0.145, 0.124, and 0.120 nm, which are characteristic of gold. The gold shell thickness was calculated to be 0.67 nm based on the weight percentage of gold in the core-shell nanoparticles (Au wt % = 38.1, determined from atomic absorption analysis) and the particle size from TEM, assuming bulk density. A negative MR was observed at 10 K. This observation is similar to the recently reported MR study in $Fe_{core}Au_{shell}$ nanoparticles by Cho et al.[12] Similar to that study, the temperature-dependent resistance, as shown in the inset of Fig. 1, reflects a positive temperature coefficient of resistance, characteristic of metallic conduction rather than the thermally activated behavior with a negative temperature co-
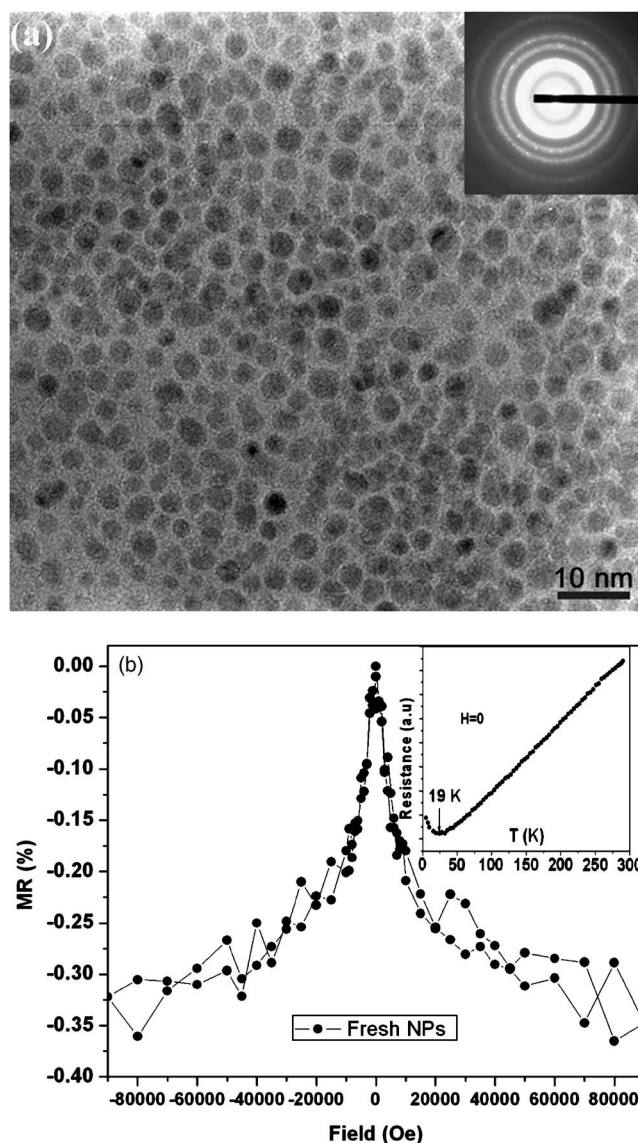

Figure 1. $Co_{core}Au_{shell}$ nanoparticles without annealing treatment: (a) TEM image and (b) MR as a function of applied field at 10 K (inset shows the temperature-dependent resistance at zero applied magnetic field).

ficient. This observation indicates that the $Co_{core}Au_{shell}$ nanoparticles are still metallic, even with the existence of the SB3–12 surfactant chemically bonded onto the surface.

Figure 2 shows the magnetic-field-dependent resistance at 10 K for the $Co_{core}Au_{shell}$ nanoparticles annealed at different temperatures. (The nomenclature $Co_{core}Au_{shell}$ is used here to depict the nanoparticles, though it is possible that alloy formation may occur, particularly at the interfacial regions upon heat-treatment). A large increase in the MR occurred when the nanoparticles were annealed at 200°C in a hydrogen environment, compared to the unannealed case (Fig. 1). An increase in the annealing temperature resulted in a lower MR and a change in the shape of the MR with the applied field. A similar metallic conduction behavior was observed for the annealed $Co_{core}Au_{shell}$ nanoparticles; a typical example at 450°C is shown in the inset of Fig. 2. The impurity-dominated region, before the transition to metallic conduction behavior, is expanded to a larger temperature range as expected from the decomposition of the surfactant. There is an increase in MR (up to 1.5%) when the sample was annealed at 200°C. The MR subsequently decreases with a further increase of the annealing temperature. This observation is
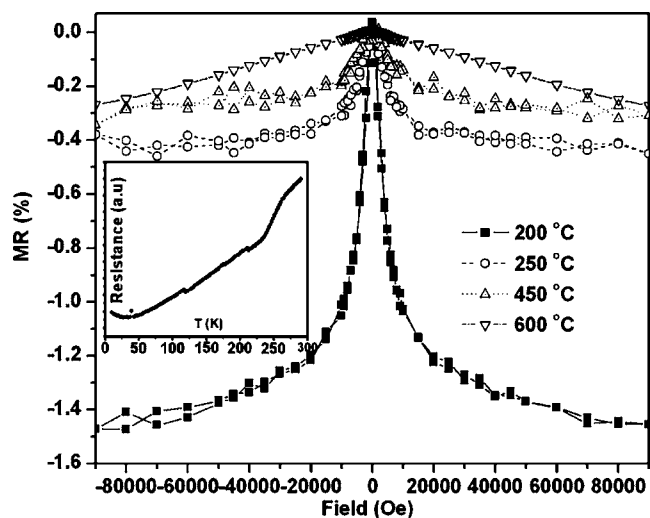
Figure 2. (a) MR as a function of applied field at 10 K for the $Co_{core}Au_{shell}$ nanoparticles annealed at 200, 250, 450, and 600°C, respectively. (Inset shows the typical temperature-dependent resistance at zero applied magnetic field.)

Figure 4. (Color online) FTIR spectra of (a) the SB3–12 and (b) SB3–12 stabilized $Co_{core}Au_{shell}$ nanoparticles, SB3–12 stabilized $Co_{core}Au_{shell}$ nanoparticles annealed at (c) 200, (d) 250, (e) 450, and (f) 600°C.

consistent with the reported melt-spun Co–Cu granular alloys, where MR increased and then decreased with annealing temperature.[21,31-33] It was reported that the maximum MR value occurred for particle diameters around the electron mean-free path,[33,34] and it is expected that the particle size and the nature of the surfactant would be affected by the annealing step.

The change of the particle size with annealing temperature is shown in Fig. 3 before compression. Figures 3a-c show TEM micrographs of the annealed $Co_{core}Au_{shell}$ nanoparticles at 200, 250, and 450°C and their corresponding selected area electron diffraction (SAED), shown in insets. Figure 3d shows a SEM image of the $Co_{core}Au_{shell}$ nanoparticles annealed at 600°C. Following annealing

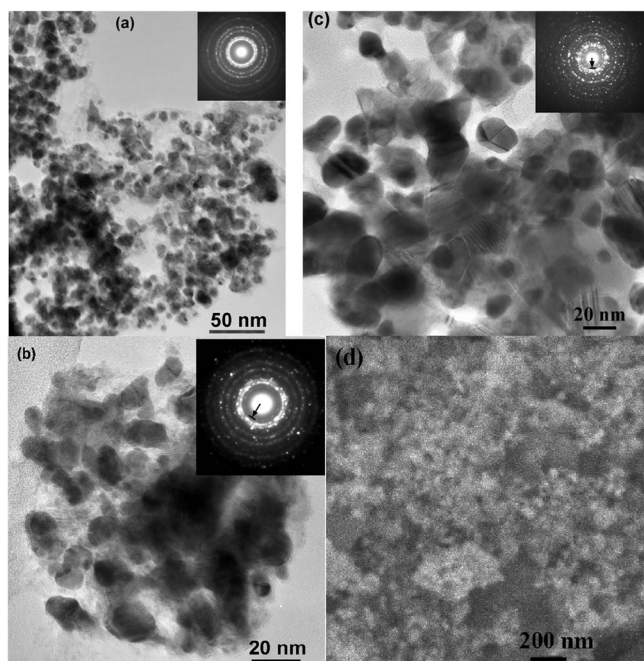**Figure 3.** TEM bright-field micrographs of $Co_{core}Au_{shell}$ nanoparticles annealed at (a) 200, (b) 250, and (c) 450°C, respectively; and (d) SEM microstructure of the $Co_{core}Au_{shell}$ nanoparticles annealed at 600°C. (Arrows indicate graphitic carbon formation.)

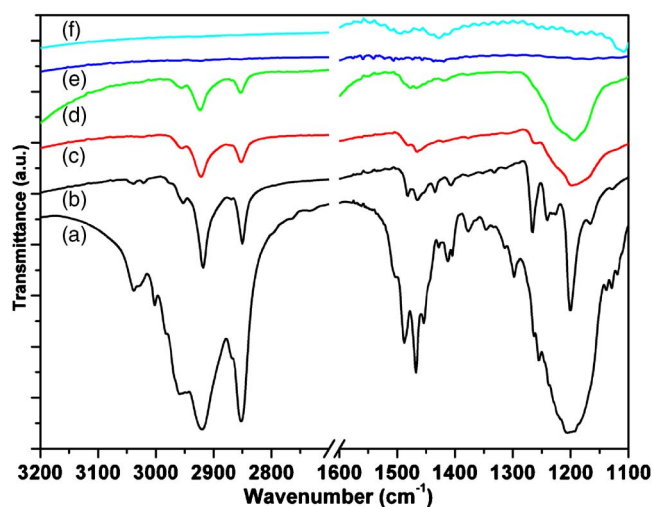the $Co_{core}Au_{shell}$ particle size increases. After 200°C, the particle has an average size of 6.7 nm with a standard deviation of 1.0 nm. The particle size was 9.1 ± 2.6 nm after annealing at 250°C. With further increase of the annealing temperature, the average particle size increased to 13.0 ± 3.6 nm and 53.3 ± 9.7 nm for the $Co_{core}Au_{shell}$ nanoparticle annealed at 450 and 600°C, respectively. For the $Co_{core}Au_{shell}$ nanoparticles annealed at 200°C, SAED rings, from inner to outer, correspond to the lattice spacings of 0.233, 0.201, 0.140, 0.121, and 0.112 nm, which are characteristic of gold. There is no carbon observation in this annealing process, indicating no decomposition of SB3–12 surfactant and consistent with the reported SB3–12 melting point (250−260°C). For $Co_{core}Au_{shell}$ nanoparticles annealed at 250°C, bright rings (from inner to outer) were observed with plane spacing of 0.233, 0.201, 0.147, 0.123, and 0.108 nm, which are again characteristic of gold. The weak inner ring is due to the formation of carbon with a calculated lattice spacing of 0.317 nm corresponding to the (002) plane of carbon. The SAED patterns for $Co_{core}Au_{shell}$ nanoparticles annealed at 450°C are similar to those of the 250°C-annealed $Co_{core}Au_{shell}$ nanoparticles. However, a significant difference is that the patterns in the 450°C-annealed sample have more spots than the 250°C-annealed sample, which reflects a more orderly crystal orientation arising from the larger size particles. The broader distribution of particle size found at the higher annealing temperatures can account for the more bell-shaped MR curve observed in Fig. 2. MR does not reach saturation even at higher applied magnetic field, which is consistent with reported granular nanomaterials.[30] A high field is necessary to align the magnetic moments of particles having various shapes and sizes due to the high anisotropy energy. At high annealing temperatures the surfactant is expected to be decomposed to a graphitic material, while at low annealing temperatures the surfactant is still present. Thus, the MR behavior may also be influenced by the presence of the surfactant and so cannot be treated as a conventional granular MR material over all the annealing temperatures.

Figure 4 shows the FTIR spectra of (a) pure SB3–12, (b) the SB3–12 stabilized $Co_{core}Au_{shell}$ nanoparticles, and (c–f) the nanoparticles following annealing. The strong bands at 2919 and 2851 cm^{-1} of the free SB3–12 surfactant are assigned to the asymmetric and symmetric CH_2 stretching modes, respectively, similar to Salker et al.[35] It was reported that the shape (narrowness and the wave number location) of the FTIR spectra was an indicator of the physicochemical interaction between the surfactant and the nanoparticles.[35,36] For pure surfactant, there are two broad bands in the region of 1540−1440 cm^{-1}. The first peak at 1488 cm^{-1} is
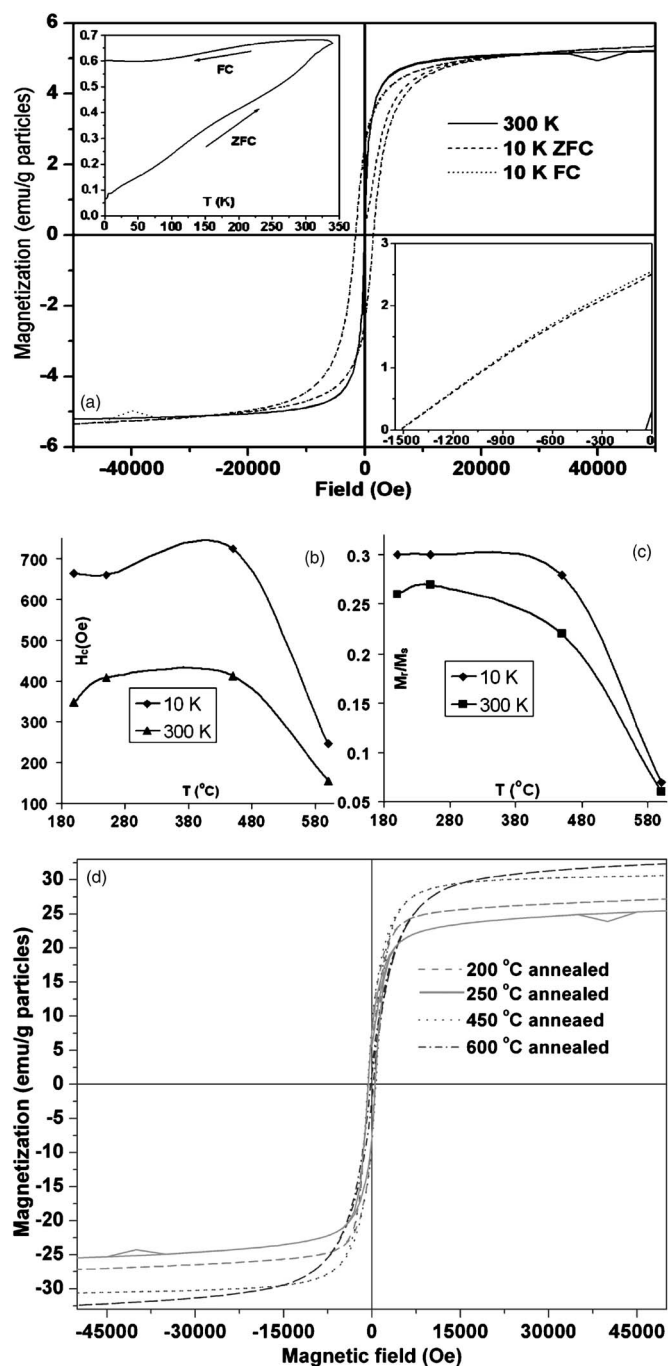
Figure 5. Field-dependent magnetization at 300 and 10 K for (a) $Co_{core}Au_{shell}$ nanoparticles without annealing (both ZFC and FC at 5 T); right and left insets show the enlarged partial $M-H$ curve, and the ZFC and FC $M-T$ curve, respectively; summary of (b) coercivity and (c) M_r/M_s ratio for the annealed samples, (d) $M-H$ hysteresis curves for the annealed samples at 10 K.

attributed to the asymmetric mode of the CH_3-(N^+) group, and the second at 1467 cm^{-1} is assigned to the CH_2 scissoring mode.[37,38] These two peaks shift to lower wavenumbers when the surfactant is coated on the nanoparticles, suggesting a less mobile environment and a strong association of these functional groups on the surface of the nanoparticles. The quaternary ammonium group coordinates to the surface of the nanoparticle and protects the nanoparticle from agglomeration.[35] The symmetric stretching mode of the S–O is observed as a bimodal broad band at around 1275 and 1150 cm^{-1}. The

narrowing of these peaks for the surfactant bound to the nanoparticles indicates the relatively lower mobility of these functional groups in the coated $Co_{core}Au_{shell}$ nanoparticle samples. Thus, the FTIR analysis indicates that the SB3–12 is still chemically bound on the nanoparticle even after undergoing the displacement reaction and THF washing process. Thus, the compressed nanoparticle–surfactant material is similar to a composite-like granular alloy. Figure 4c-f shows the spectra of the annealed nanoparticles at different temperatures (200, 250, 450, and 600°C). The spectrum of the SB3–12 bound on the $Co_{core}Au_{shell}$ nanoparticles after being annealed at lower temperature (200 and 250°C) exhibits the characteristic peaks of SB3–12. This indicates the presence of the SB3–12 surfactant even after a 2 h annealing process. There is a disappearance of the peaks for the samples annealed at 450 and 600°C, indicating the complete decomposition of the surfactant. This observation is consistent with the electron diffraction rings of the TEM in Fig. 3 and is consistent with the expected melting point of SB3–12 (250–260°C). There is an additional SAED ring in Fig. 3b and c annealed at 250 and 450°C compared to the lower temperature annealing at 200°C, as indicated by arrows in the figures. The location of the ring suggests a large d-spacing characteristic of graphitic carbon.

Figure 5 shows the magnetic property of the fresh $Co_{core}Au_{shell}$ nanoparticles and the annealed samples. The coercivity and remnant magnetization are the axes interception points of the hysteresis plot. In Fig. 5a, the temperature-dependent magnetization curve under ZFC and FC conditions at 100 Oe shows that the blocking temperature (T_B), characteristic of the transition temperature between the superparamagnetic state and the ferromagnetic state, is above room temperature. The high T_B was further evidenced by the nonzero coercivity (H_c) and remnant magnetization (M_r), as shown in the right inset. A large T_B is contrary to what is expected from uncapsulated nanoparticles. In an earlier report[10] it was observed that Co nanoparticles displaced by Cu ions to form a Cu shell increased the blocking temperature of the nanoparticles, despite the smaller Co core. Similarly, here, the Au shell has increased the blocking temperature. In order to test the presence of the CoO impurities in core-shell nanoparticles, the samples were cooled from 300 to 10 K with an applied field of 5 T. It was reported that exchange interaction between the ferromagnetic (FM) and antiferromagnetic (AFM) regions gave rise to the shifted hysteresis loop along the field direction after FC procedures.[39-41] The FC hysteresis loop is shown in Fig. 5 with the ZFC hysteresis loop as comparison. The almost overlapping of the ZFC and FC hysteresis loops in the unannealed sample (top plot) indicates that oxidation formation could be avoided during the cobalt precursor nanoparticle synthesis, displacement reaction process, and sample preparation. Figure 5b shows the magnetic properties of the annealed $Co_{core}Au_{shell}$ nanoparticles at different temperatures. The nonzero values of H_c and M_r for all the annealed nanoparticle samples indicate that the annealed nanoparticles are ferromagnetic. Coercivity (H_c) increases and then decreases with a change in the annealing temperature. The H_c for the as-prepared core–shell nanoparticles are 1521 Oe at 10 K and 36 Oe at 300 K. The as-prepared core–shell nanoparticles have a significantly larger H_c than all the annealed samples at 10 K but have a significantly lower value at room temperature. The increase in H_c trend is expected with an increase of the particle size observed in Fig. 3 after the annealing process. The increase continues until the critical size for the single domain particles is reached; then H_c decreases. This observation is consistent with the annealing effect observation on the coercivity of the $Co_{100-x}Cu_x$ alloys.[21,42] The ratio of the remnant magnetization (M_r) to the saturation magnetization (M_s), or squareness, decreases with an increase of the annealing temperature. The M_r/M_s for the as-prepared core–shell nanoparticles are similar to the slightly annealed conditions at 200°C at 10 K but significantly lower at 300 K. Both H_c and M_r/M_s are higher at the lower measuring temperature, which is expected from the reduced thermal energy. Figure 5d shows the $M-H$ plots at 10 K as a rep-

resentative example of the annealed samples. At an annealed temperature of 600°C, the sample M_s does not saturate at low field, consistent with the MR bell-shaped curve in Fig. 2.

Conclusion

Compressed $Co_{core}Au_{shell}$ nanoparticles prepared by a displacement reaction with a SB3–12 surfactant were shown to exhibit MR. The surfactant was chemically bound to the nanoparticles as indicated by FTIR, and thus the resulting material is a composite together with nanoparticles and surfactant. The annealing effect on the microstructure, magnetic properties, physicochemical interaction between the SB3–12 and the core–shell nanoparticles was investigated and was found to alter dramatically the particles and resulting magnetic properties. An annealing step at a temperature below the melting point of the surfactant resulted in the largest MR. Higher temperature decomposed the surfactant concomitant with larger particle sizes. Coercivity increased and then decreased with the augmentation of the annealing temperature, while the ratio of the remnant magnetization to saturation magnetization decreased.

Acknowledgments

References

1. V. F. Puntes, K. M. Krishnan, and A. P. Alivisatos, *Science*, **291**, 2115 (2001).
2. S. H. Sun and C. B. Murray, *J. Appl. Phys.*, **85**, 4325 (1999).
3. K. J. Klabunde, D. Zhang, G. N. Glavee, C. M. Sorensen, and G. C. Hadjipanayis, *Chem. Mater.*, **6**, 784 (1994).
4. L. A. Harris, J. D. Goff, A. Y. Carmichael, J. S. Riffle, J. J. Harburn, T. G. St. Pierre, and M. Saunders, *Chem. Mater.*, **15**, 1367 (2003).
5. S. Sun, C. B. Murray, D. Weller, L. Folks, and A. Moser, *Science*, **287**, 1989 (2000).
6. E. J. Podlaha, Y. Li, J. Zhang, Q. Huang, A. Panda, A. Lozano-Morales, D. Davis, and Z. Guo, *Nanomaterials Handbook*, pp. 475–495, CRC Press, Taylor & Francis Group, Boca Raton, FL (2006).
7. M. Chen, S. Yamamuro, D. Farrell, and S. A. Majetich, *J. Appl. Phys.*, **93**, 7551 (2003).
8. Y. Qiang, J. Antony, M. Marino, and S. Pendyala, *IEEE Trans. Magn.*, **40**, 3538 (2004).
9. J.-I. Park and J. Cheon, *J. Am. Chem. Soc.*, **123**, 5743 (2001).
10. Z. Guo, C. Kumar, L. L. Henry, E. E. Doomes, J. Hormes, and E. J. Podlaha, *J.*
11. Z. Lu, M. D. Prouty, Z. Guo, V. O. Golub, C. Kumar, and Y. M. Lvov, *Langmuir*, **21**, 2042 (2005).
12. S.-J. Cho, S. M. Kauzlarich, J. Olamit, K. Liu, F. Grandjean, L. Rebbouh, and G. J. Long, *J. Appl. Phys.*, **95**, 6804 (2004).
13. S. U. Son, Y. Jang, J. Park, H. B. Na, H. M. Park, H. J. Yun, J. Lee, and T. Hyeon, *J. Am. Chem. Soc.*, **126**, 5026 (2004).
14. Z. Guo, C. Kumar, L. L. Henry, C. K. Saw, J. Hormes, and E. J. Podlaha, Abstracts of the 49th Magnetic and Magnetic Materials (MMM) Annual Conference, p. 366 (2004).
15. J. Lin, W. Zhou, A. Kumbhar, J. Wiemann, J. Fang, E. E. Carpenter, and C. J. O'Connor, *J. Solid State Chem.*, **159**, 26 (2001).
16. Y. Bao, H. Calderon, and K. M. Krishnan, *J. Phys. Chem. C*, **111**, 1941 (2007).
17. D. A. Fleming, M. Napolitano, and M. E. Williams, *Mater. Res. Soc. Symp. Proc.*, **746**, 207 (2003).
18. C. A. Ross, *Annu. Rev. Mater. Sci.*, **24**, 159 (1994).
19. S. S. P. Parkin, *Annu. Rev. Mater. Sci.*, **25**, 357 (1995).
20. A. Fert and L. Piraux, *J. Magn. Magn. Mater.*, **200**, 338 (1999).
21. R. Yu, X. Zhang, J. Tejada, J. Zhu, and M. Knobel, *J. Appl. Phys.*, **79**, 1979 (1996).
22. S. Zhang and P. M. Levy, *J. Appl. Phys.*, **73**, 5315 (1993).
23. T. A. Rabedeau, M. F. Toney, R. F. Marks, S. S. P. Parkin, R. F. C. Farrow, and G. R. Harp, *Phys. Rev. B*, **48**, 16810 (1993).
24. M. Zhuravlev, H. Lutz, and A. V. Vedyayev, *Phys. Rev. B*, **63**, 174409 (2001).
25. A. Berkowitz, J. Mitchell, M. Carey, A. Young, D. Rao, A. Starr, S. Zhang, F. Spada, F. Parker, A. Hutten, and G. Thomas, *J. Appl. Phys.*, **73**, 5320 (1993).
26. T. Koide, H. Miyauchi, J. Okamoto, T. Shidara, A. Fujimori, H. Fukutani, K. Amemiya, H. Takeshita, S. Yuasa, T. Katayama, and Y. Suzuki, *Phys. Rev. Lett.*, **87**, 257201 (2001).
27. D. Kahn, in *Proceedings of the 79th AESF Annual Technical Conference*, p. 305–341 (1992).
28. Y. Okinaka and M. Hoshino, *Gold Bull.*, **31**, 3 (1998).
29. M. Guan, Ph.D. Thesis, Louisiana State University, Baton Rouge, LA (2005).
30. A. Fert, A. Barthelemy, P. Galtier, P. Holody, R. Loloee, R. Morel, F. Petroff, P. Schroeder, L. B. Steren, and T. Valet, *Mater. Sci. Eng., B*, **31**, 1 (1995).
31. A. Garcia Prieto, M. L. Fdez–Gubieda, C. Meneghini, A. Garcia-Arribas, and S. Mobilio, *Phys. Rev. B*, **67**, 224415 (2003).
32. A. D. C. Viegas, J. Geshev, L. S. Dorneles, J. E. Schmidt, and M. Knobel, *J. Appl. Phys.*, **82**, 3047 (1997).
33. D. Kechrakos and K. N. Trohidou, *Phys. Rev. B*, **62**, 3941 (2000).
34. J. Q. Xiao, J. S. Jiang, and C. L. Chien, *Phys. Rev. Lett.*, **68**, 3749 (1992).
35. R. A. Salkar, P. Jeevanandam, G. Kataby, S. T. Aruna, Y. Koltypin, O. Palchik, and A. Gedanken, *J. Phys. Chem. B*, **104**, 893 (2000).
36. Y. Sahoo, H. Pizem, T. Fried, D. Golodnitsky, L. Burstein, C. N. Sukenik, and G. Markovich, *Langmuir*, **17**, 7907 (2001).
37. R. G. Snyder, *J. Mol. Spectrosc.*, **7**, 116 (1961).
38. J. Umemura, D. Cameron, and H. Mantsch, *Biochim. Biophys. Acta*, **602**, 32 (1980).
39. S. Gangopadhyay, G. C. Hadjipanayis, C. M. Sorensen, and K. J. Klabunde, *J. Appl. Phys.*, **73**, 6964 (1993).
40. D. L. Peng, K. Sumiyama, T. Hihara, S. Yamamuro, and T. J. Konno, *Phys. Rev. B*, **61**, 3103 (2000).
41. M. Verelst, T. O. Ely, C. Amiens, E. Snoeck, P. Lecante, A. Mosset, M. Respaud, J. M. Broto, and B. Chaudret, *Chem. Mater.*, **11**, 2702 (1999).
42. S. Ram and P. S. Frankwicz, *Phys. Status Solidi A*, **188**, 1129 (2001).

Electrochem. Soc., **152**, D1 (2005).